Theory of magnetic neutron spectroscopy for Pr^{3+} and Tm^{3+}

1992 J. Phys.: Condens. Matter 4 2271

(http://iopscience.iop.org/0953-8984/4/9/021)

J. Phys.: Condens. Matter 4 (1992) 2271–2280. Printed in the UK

Theory of magnetic neutron spectroscopy for Pr^{3+} and Tm^{3+}

Ewald Balcar† and Stephen W Lovesey§

† Atomic Institute of the Austrian Universities, A-1020 Vienna, Austria
§ Rutherford Appleton Laboratory, Oxfordshire OX11 0QX, UK

Received 1 October 1991

Abstract. Motivated by recent data on the strongly inelastic magnetic neutron scattering spectrum of praseodymium and thulium metal, over a wide range of energy and wave vector κ transfers, we have calculated the corresponding spectrum for both ions and the κ-dependence of the relevant inelastic structure factors. The model includes the seven lowest energy states and their mixing by the spin–orbit coupling: results differ from previous calculations for the f^2/f^{12} state and this is attributed to mixed phase conventions for the base states used for the representation of the spin–orbit energy matrix and the magnetic neutron interaction. Comparison of results from the correct model with existing neutron beam data shows satisfactory agreement; remaining discrepancies are attributed to potentially interesting shortcomings of an isolated ion model for rare earth metals. The unintentional exercise of using correct and incorrect wave functions underlines the sensitivity of inelastic structure factors to features of the magnetic wave functions.

1. Introduction

The study of atomic states by probing their properties with neutrons has been significantly advanced through use of intense and pulsed neutron beams from modern spallation sources. With energy transfers currently up to 2 eV a new range of states in magnetic ions becomes susceptible to investigation. Neutron spectroscopy complements optical experiments by allowing non-dipole transitions at finite wave vector transfers and is the method of choice for optically non-transparent materials.

For rare earth metals and compounds a realistic model is provided by an isolated magnetic ion. In the following work, structure factors are derived for electrons in a 4f configuration. It is the deviation between this model and experimental data which might then lead to further understanding of electronic states.

2. Atomic states

Several rare earth ions have been studied by neutron spectroscopy [1]. In this paper we concentrate our attention on praseodymium and thulium in a triply ionized ionic state, corresponding to electron configurations of f^2 and f^{12}, respectively. The wave functions cited in [2] for the calculation of magnetic neutron scattering have been used under incorrect assumptions for the treatment of magnetic neutron scattering: the root of the error is mixing of phase conventions. In order to perform a consistent

0953-8984/92/092271+10$04.50

discussion, not only of the magnetic scattering but also of the spin–orbit interaction mixing the Russell–Saunders states with equal J, we resort to the general apparatus of Racah algebra and tensor operators. The atomic states belonging to a J-multiplet are built from Russell–Saunders, or LS-states, coupled with Clebsch–Gordan coefficients,

$$|vSLJM\rangle = \sum_{M_S M_L} (SM_S LM_L|JM)|vSM_S LM_L\rangle \tag{1}$$

where v is a quantum label, e.g. seniority. Note also that we customarily refer to 'LS-states' although the actual coupling order in (1) is the other way round. By virtue of the Wigner–Eckart theorem the matrix elements of a spherical tensor operator X_Q^K of rank K may be split into two parts, one of which, the reduced matrix element, does not depend on the magnetic quantum numbers; the remaining part is given by a phase factor and a $3j$ symbol,

$$\langle vSLJM|X_Q^K|v'S'L'J'M'\rangle = (-1)^{J-M}\begin{pmatrix} J & K & J' \\ -M & Q & M' \end{pmatrix}(vSLJ\|X^K\|v'S'L'J') \tag{2}$$

In (2) and the remaining work we adhere to the definitions used by Edmonds [3] and Judd [4].

If we assume that the spherical tensor X_Q^K is built from two tensors U_γ^κ and V_q^k, which operate, quite generally, on the spin and orbital part of the wave functions, respectively,

$$X_Q^K = \{U_\gamma^\kappa \otimes V_q^k\}_Q^K \equiv \sum_{q,q'} U_\gamma^\kappa V_q^k (\kappa\gamma kq|KQ) \tag{3}$$

the many-electron reduced matrix element $(vSLJ\|X^K\|v'S'L'J')$ can be written in a very compact fashion with the help of a unit tensor $W^{(\kappa,k)K}$,

$$(vSLJ\|X_Q^K\|v'S'L'J') = (s\|u^\kappa\|s)(l\|v^k\|l)(\theta J\|W^{(\kappa,k)K}\|\theta' J') \tag{4}$$

Here $(s\|u^\kappa\|s)$ and $(l\|v^k\|l)$ are the one-electron reduced matrix elements of the spin and orbital operators in U and V, respectively, and θ, θ' are abbreviations for $vSL, v'S'L'$. The main effort necessary in the treatment of matrix elements of many-electron wave functions is concentrated in the calculation of the reduced matrix element $(\theta J\|W^{(\kappa,k)K}\|\theta' J')$. The more widely used double unit tensor $W^{(\kappa,k)}$ is related to the quantity used in (4) by a $9j$-symbol and, following Judd [4],

$$(\theta J\|W^{(\kappa,k)K}\|\theta' J') = \sqrt{\frac{(2J+1)(2K+1)(2J'+1)}{(2\kappa+1)(2k+1)}}\begin{Bmatrix} S & L & J \\ S' & L' & J' \\ \kappa & k & K \end{Bmatrix}(\theta\|W^{(\kappa,k)}\|\theta'). \tag{5}$$

Similar unit tensors $U^{(k)}$ and $V^{(1,1)}$ have been introduced by Racah [5] and their reduced matrix elements were tabulated for various l^n by Nielson and Koster [6]. These are closely related to the quantities used here; in fact

$$(\theta\|W^{(1,1)}\|\theta') = \sqrt{6}(\theta\|V^{(1,1)}\|\theta') \qquad (\theta\|W^{(0,k)}\|\theta') = \sqrt{\frac{(2S+1)(2k+1)}{2}}(\theta\|U^{(k)}\|\theta'). \tag{6}$$

In accordance with the value of $\kappa + k$ we discriminate between even and odd unit tensor operators $W^{(\kappa,k)}$, which have remarkable properties [5, 7]. Since we intend to apply our formalism to the spin–orbit interaction, we consider $\kappa + k$ =even and find for $\nu = \nu'$, $\Delta\nu = 0, \pm 2$,

$$(l^n v S L \| W^{(\kappa,k)} \| l^n v S' L') = \left(\frac{2l+1-n}{2l+1-v}\right)(l^v v S L \| W^{(\kappa,k)} \| l^v v S' L'). \tag{7}$$

The reduced matrix element, in this case, changes its sign for a conjugate state l^{4l+2-n} for which there are common quantum numbers, including seniority. The analogue for $\kappa + k$ =odd is

$$(l^n v S L \| W^{(\kappa,k)} \| l^n v' S' L') = \delta_{vv'}(l^v v S L \| W^{(\kappa,k)} \| l^v v' S' L'). \tag{8}$$

Thus, odd unit tensors, which are relevant to the description of magnetic neutron scattering, have equal reduced matrix elements for conjugate states.

3. Spin–orbit interaction

In order to treat the matrix elements of the spin–orbit interaction we have rewritten the usual form of $\mathcal{H}_{SO}$ within the framework sketched above,

$$\mathcal{H}_{SO} = \sum_{\nu} s_\nu \cdot l_\nu = (-1)\sqrt{3}\{s_q^1 \otimes l_q^1\}_0^0 \tag{9}$$

such that the coupling of two spherical tensor operators, spin and orbital momentum, to a tensor of rank 0 is manifest. With ($l = 3$, $s = \frac{1}{2}$)

$$(l\|l\|l) = \sqrt{l(l+1)(2l+1)} = 2\sqrt{21} \tag{10}$$

$$(s\|s\|s) = \sqrt{s(s+1)(2s+1)} = \sqrt{\frac{3}{2}} \tag{11}$$

we arrive at an expression for the reduced matrix element of $\mathcal{H}_{SO}$:

$$(v S L J \| \mathcal{H}_{SO} \| v' S' L' J) = 6\sqrt{\frac{7}{2}}(v S L J \| W^{(1,1)0} \| v' S' L' J')\delta_{J,J'}. \tag{12}$$

The relevant reduced matrix elements of the unit tensor $W^{(1,1)0}$ are given in table 1 for the terms and J-values belonging to a f^2/f^{12} configuration.

For the complete matrix element of $\mathcal{H}_{SO}$ we need a $3j$-symbol which turns out to be very simple and independent of M,

$$(-1)^{J-M}\begin{pmatrix} J & 0 & J \\ -M & 0 & M \end{pmatrix} = \frac{1}{\sqrt{2J+1}} \quad . \tag{13}$$

As an example, we give the non-zero matrix elements of $\mathcal{H}_{SO}$ for J=4, which are independent of M:

$$\langle {}^3H_4|\mathcal{H}_{SO}|{}^3H_4\rangle = -3 \qquad \langle {}^3H_4|\mathcal{H}_{SO}|{}^1G_4\rangle = -\sqrt{\frac{10}{3}}$$

$$\langle {}^3F_4|\mathcal{H}_{SO}|{}^3F_4\rangle = \frac{3}{2} \qquad \langle {}^3F_4|\mathcal{H}_{SO}|{}^1G_4\rangle = \sqrt{\frac{11}{3}}.$$

Table 1. Reduced matrix elements $(\theta J\|W^{(1,1)0}\|\theta' J')$ for the LS-terms occurring in an f^2/f^{12} configuration.

	$^1I_6$	$^3H_6$	$^3H_5$	$^3H_4$	$^1G_4$	$^3F_4$	$^3F_3$
β^1I_6	0	$-\frac{1}{6}\sqrt{\frac{13}{7}}$					
$^3H_6$	$-\frac{1}{6}\sqrt{\frac{13}{7}}$	$-\frac{5}{6}\sqrt{\frac{13}{42}}$					
$^3H_5$			$\frac{1}{6}\sqrt{\frac{11}{42}}$				
$^3H_4$				$\sqrt{\frac{3}{14}}$	$\frac{1}{3}\sqrt{\frac{5}{7}}$	0	
$^1G_4$				$\frac{1}{3}\sqrt{\frac{5}{7}}$	0	$-\frac{1}{3}\sqrt{\frac{11}{14}}$	
$^3F_4$				0	$-\frac{1}{3}\sqrt{\frac{11}{14}}$	$-\frac{1}{2}\sqrt{\frac{3}{14}}$	
$^3F_3$							$\frac{1}{6}\sqrt{\frac{1}{6}}$

	$^3F_2$	$^1D_2$	$^3P_2$	$^3P_1$	$^3P_0$	$^1S_0$
β^3F_2	$\frac{1}{3}\sqrt{\frac{10}{21}}$	$\frac{1}{3}\sqrt{\frac{5}{7}}$	0			
$^1D_2$	$\frac{1}{3}\sqrt{\frac{5}{7}}$	0	$-\frac{1}{2}\sqrt{\frac{5}{21}}$			
$^3P_2$	0	$-\frac{1}{2}\sqrt{\frac{5}{21}}$	$-\frac{1}{6}\sqrt{\frac{5}{42}}$			
$^3P_1$				$\frac{1}{6}\sqrt{\frac{1}{14}}$		
$^3P_0$					$\frac{1}{3}\sqrt{\frac{1}{42}}$	$\frac{1}{3}\sqrt{\frac{2}{7}}$
$^1S_0$					$\frac{1}{3}\sqrt{\frac{2}{7}}$	0

The complete set of matrix elements of $\mathcal{H}_{SO}$ is given in table 2. If we compare the values listed in this table with the corresponding values given by Satten and Margolies [8], some of the off-diagonal elements, namely $\langle^3H_4|\mathcal{H}_{SO}|^1G_4\rangle$, $\langle^1D_2|\mathcal{H}_{SO}|^3P_2\rangle$, and $\langle^3P_0|\mathcal{H}_{SO}|^1S_0\rangle$, carry a different sign. This can be traced back to a different phase convention used in [8] for the definition of some basis states, i.e. ^1G, ^3F, ^1D, and ^1S. These states are chosen with a different phase in [8] compared to our choice, which follows Judd [4] and Edmonds [3]. These different phases have no influence on the energy values for the 13 states of Pr^{3+} resulting from a diagonalization of both the spin–orbit interaction and the Coulomb interaction. The eigenstates, however, are directly affected by the phases chosen.

In figure 1 we plot the energy dependence of the low-lying LS-states, $^3H_{4,5,6}$, $^3F_{2,3,4}$, and $^1G_4$, under the influence of spin–orbit interactions with strength in the range from 0 to 200 meV. The dotted curves are drawn parallel to the ground state energy at those relative energy transfers as determined by measurement [2]. Except for the transition to $^3H_6$, which is too weak to be measured, all other levels can be seen to intersect the dotted curves at a spin–orbit strength ζ of 92 meV. In view of this, subsequent calculations for Pr^{3+} were made with $\zeta=92$ meV and the states corresponding to this interaction strength are listed in table 3.

A similar set of curves, in the range from 0 to −400 meV, describes in figure 2 the variation of level energies with increasing (negative) spin–orbit interaction for the conjugate configuration. The state with lowest energy starts as $^3H_6$, in this case, and acquires a small admixture of $^1I_6$. From figure 2 we see that the measured energies

Table 2. Matrix elements of the spin–orbit interaction $\mathcal{H}_{SO}$ for the LS-terms of a f^2/f^{12} configuration. The entries have to be multiplied with the spin–orbit interaction strength ζ, namely 92 meV and -327 meV for Pr^{3+} and Tm^{3+}, respectively.

	$^1I_6$	$^3H_6$	$^3H_5$	$^3H_4$	$^1G_4$	$^3F_4$	$^3F_3$	$^3F_2$	$^1D_2$	$^3P_2$	$^3P_1$	$^3P_0$	$^1S_0$
$^1I_6$	0	$\sqrt{\frac{3}{2}}$											
$^3H_6$	$\sqrt{\frac{3}{2}}$	$\frac{5}{2}$											
$^3H_5$			$-\frac{1}{2}$										
$^3H_4$				-3	$-\sqrt{\frac{10}{3}}$	0							
$^1G_4$				$-\sqrt{\frac{10}{3}}$	0	$\sqrt{\frac{11}{3}}$							
$^3F_4$				0	$\sqrt{\frac{11}{3}}$	$\frac{3}{2}$							
$^3F_3$							$-\frac{1}{2}$						
$^3F_2$								-2	$-\sqrt{6}$	0			
$^1D_2$								$-\sqrt{6}$	0	$\frac{3}{2}\sqrt{2}$			
$^3P_2$								0	$\frac{3}{2}\sqrt{2}$	$\frac{1}{2}$			
$^3P_1$											$-\frac{1}{2}$		
$^3P_0$												-1	$-\sqrt{12}$
$^1S_0$												$-\sqrt{12}$	0

Table 3. Seven low-lying LS-states of Pr^{3+} and their corresponding linear combinations arising from a spin–orbit interaction ζ=92 meV. The states are ordered with ascending energy.

$^3H_4$	→	$0.985\ ^3H_4 + 0.168\ ^1G_4 - 0.032\ ^3F_4$
$^3H_5$	→	$^3H_5$
$^3H_6$	→	$0.998\ ^3H_6 - 0.059\ ^1I_6$
$^3F_2$	→	$0.988\ ^3F_2 + 0.157\ ^1D_2 - 0.015\ ^3P_2$
$^3F_3$	→	$^3F_3$
$^3F_4$	→	$0.125\ ^3H_4 - 0.580\ ^1G_4 + 0.805\ ^3F_4$
$^1G_4$	→	$-0.117\ ^3H_4 + 0.797\ ^1G_4 + 0.592\ ^3F_4$

[1] coincide with the calculated levels for $\zeta = -327$ meV. The states resulting from a diagonalization of Coulomb and spin–orbit interaction are listed in table 4.

Table 4. Seven low-lying LS-states of Tm^{3+} and their corresponding linear combinations arising from a spin–orbit interaction $\zeta = -327$ meV. The states are ordered with ascending energy.

$^3H_6$	→	$0.996\ ^3H_6 + 0.092\ ^1I_6$
$^3F_4$	→	$-0.297\ ^3H_4 + 0.568\ ^1G_4 + 0.767\ ^3F_4$
$^3H_5$	→	$^3H_5$
$^3H_4$	→	$0.754\ ^3H_4 - 0.353\ ^1G_4 + 0.553\ ^3F_4$
$^3F_3$	→	$^3F_3$
$^3F_2$	→	$0.890\ ^3F_2 - 0.439\ ^1D_2 - 0.123\ ^3P_2$
$^1G_4$	→	$0.585\ ^3H_4 + 0.743\ ^1G_4 - 0.324\ ^3F_4$

The main difference to previous results occurs with respect to the eigenstates. Since the spin–orbit interaction mixes states with the same angular momentum J,

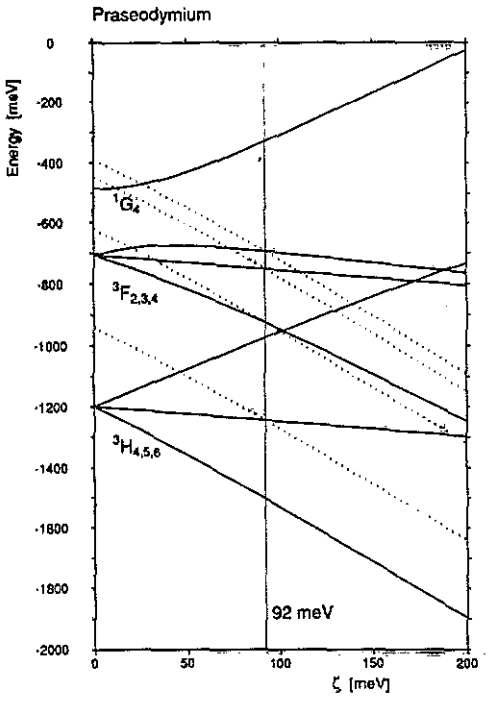

Figure 1. Energy levels of the seven lowest states of Pr^{3+} as they develop from $^3H_{4,5,6}$, $^3F_{2,3,4}$, and $^1G_4$ with increasing spin–orbit interaction. The dotted graphs are drawn at relative distances of 259, 577, 751, and 808 meV, respectively, from the ground state, as measured in [2].

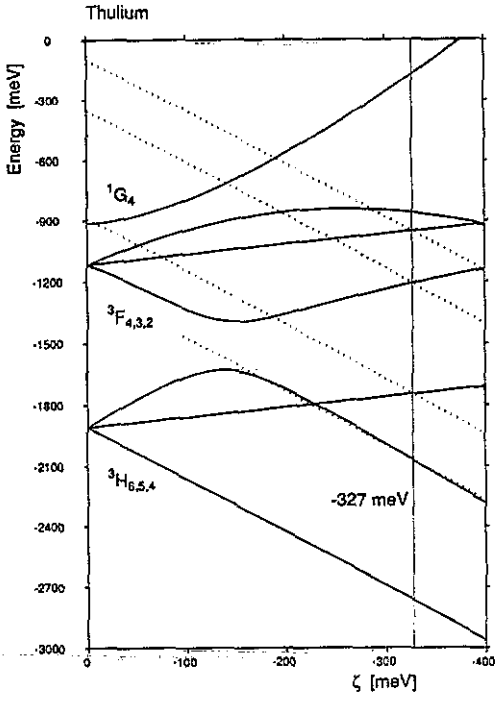

Figure 2. Energy levels of the seven lowest states of Th^{3+} as they develop from $^3H_{6,5,4}$, $^3F_{4,3,2}$, and $^1G_4$ with increasing spin–orbit interaction. The dotted graphs are drawn at relative distances of 684, 1018, 1560, and 1760 meV, respectively, from the ground state, as measured in [1].

we expect to see this effect amongst the three states with $J = 4$ and with $J = 2$, and also for the pairs of states with $J = 6$ and $J = 0$, respectively. Restricting our attention to the range of energies accessible in an experiment, only the lowest seven states have been listed in tables 3 and 4 for Pr^{3+} and the conjugate ion Tm^{3+}.

The preceding discussion has been set up within the framework of the SL-coupling scheme. However, as shown in a recent paper by the authors [9], the theory of magnetic neutron scattering can also be expressed in the jj-scheme. Both sets of states may be used to describe the atomic states required for a realistic model of intermediate coupling. Since one of our aims was to remove the discrepancy with respect to the spin–orbit interaction matrix elements of [8], the SL-coupling scheme was our prime choice to facilitate comparison.

4. Magnetic intensities

The intensities of inelastic transitions, induced by magnetic neutron scattering, between the ground state, mainly $^3H_4$ for Pr^{3+} and $^3H_6$ for Tm^{3+}, and the states listed in tables 3 and 4, respectively, are described by a structure factor $\mathcal{G}(\kappa, \lambda, \lambda')$ as

defined in

$$\frac{d^2\sigma}{d\Omega\, dE'} = r_0^2 \frac{k'}{k} \mathcal{G}(\kappa, \lambda, \lambda')\, \delta(\hbar\omega - E_{\lambda'} - E_{\lambda}) \tag{14}$$

where $r_0 = (\gamma e^2/m_e c^2)$ is a convenient measure of magnetic scattering lengths, $\kappa = \mathbf{k} - \mathbf{k}'$, with $\mathbf{k}$, $\mathbf{k}'$ and λ, λ' referring to the initial and final neutron wave vectors and target states, respectively. The theory related to the calculation of $\mathcal{G}(\kappa, \lambda, \lambda')$ has been covered in detail in the literature; see [1, 9, 10].

Table 5. Spherical average of the cross section for magnetic scattering from the respective ground state to the same and to other spin–orbit multiplets (intra- and inter-multiplet transitions) of Pr^{3+} and Tm^{3+} expressed through radial averages of spherical Bessel functions $\langle j_K \rangle$.

	$\langle j_0 \rangle^2$	$\langle j_0 \rangle\langle j_2 \rangle$	$\langle j_2 \rangle^2$	$\langle j_2 \rangle\langle j_4 \rangle$	$\langle j_4 \rangle^2$	$\langle j_4 \rangle\langle j_6 \rangle$	$\langle j_6 \rangle^2$
			Praseodymium: Pr^{3+}				
$^3H_4$	2.164	7.285	6.152	0.069	0.068	0.166	0.751
$^3H_5$	0.194	−0.294	0.314	−0.011	0.086	−0.005	0.392
$^3H_6$	0.000	0.000	0.000	−0.002	0.070	0.007	0.220
$^3F_2$	0.000	0.000	0.141	0.482	0.650	0.078	0.335
$^3F_3$	0.000	0.003	0.107	0.034	0.202	0.023	0.340
$^3F_4$	0.003	0.014	0.196	0.005	0.061	−0.055	0.832
$^1G_4$	0.001	0.007	0.092	0.003	0.005	0.011	0.039
			Thulium: Tm^{3+}				
$^3H_6$	9.514	12.528	4.214	0.057	0.424	0.133	0.374
$^3H_5$	0.138	−0.188	0.202	−0.024	0.118	−0.006	0.246
$^3H_4$	0.000	0.000	0.161	0.055	0.070	0.035	0.339
$^3F_4$	0.000	0.000	0.758	0.528	0.209	0.024	0.808
$^3F_3$	0.000	0.000	0.004	−0.013	0.151	−0.019	0.348
$^3F_2$	0.000	0.000	0.000	0.000	0.190	−0.022	0.416
$^1G_4$	0.000	0.000	0.081	−0.010	0.033	0.002	0.040

The results contained in table 5 are for the cross section averaged over the directions of κ and they express the magnetic intensities for the various transitions through averages $\langle j_K \rangle$ of spherical Bessel functions

$$\langle j_K(\kappa) \rangle_t = \int_0^\infty dr\, r^2\, R_t^2(r)\, j_K(\kappa r) \tag{15}$$

calculated with radial parts $R_l(r)$ of f-electron wave functions. The κ-dependence of magnetic scattering intensities is thus determined both by the coefficients listed in table 5 and the κ-dependence of the $\langle j_K \rangle$.

For a numerical evaluation of magnetic intensities we have used analytical expansions for the $\langle j_K \rangle$ derived, in the case of Pr^{3+}, from non-relativistic Hartree–Fock calculations [11, 12] since relativistic data for Pr are not available [13, 14]. In order to obtain an estimate of the changes to be expected from a relativistic treatment of the electron wave functions we have compared the analytic expansions of the $\langle j_K \rangle$

for neodymium, derived from non-relativistic and relativistic data, respectively. In general, the relativistic calculation shifts weight in κ-space from high to low wavevector transfers corresponding to an expansion of the radial wave function in r-space. Above $\kappa \approx 8$ Å^{-1} the reduction for the $\langle j_K \rangle$ is at most 10%, while increases at lower κ may reach up to 20%; these effects are within the quality of the data sets. In the case of Tm^{3+} the analytic expansion used to represent the $\langle j_K \rangle$ is based on a relativistic Dirac–Fock calculation [13, 14].

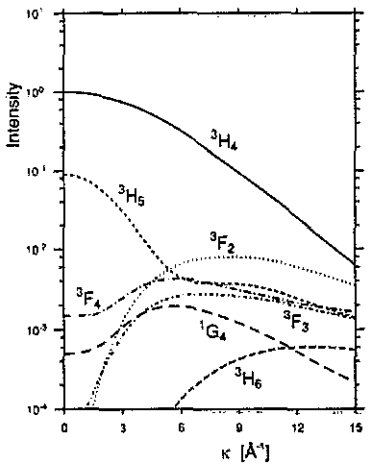

Figure 3. Intensities for magnetic neutron scattering for intra- and inter-multiplet transitions Pr^{3+}. The curves are labelled by the term dominant in the spin–orbit state.

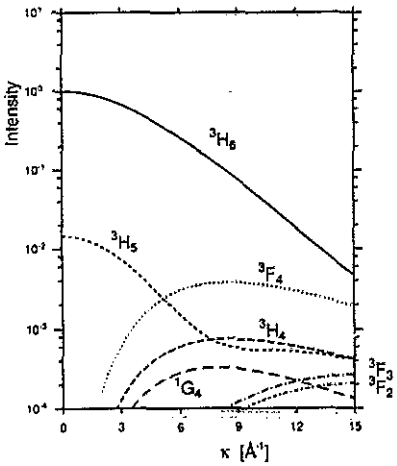

Figure 4. Intensities for magnetic neutron scattering for intra- and inter-multiplet transitions Tm^{3+}. The curves are labelled by the term dominant in the spin–orbit state.

In figure 3 we display the wave vector dependence of the magnetic intensities for transitions between the ground state of Pr^{3+} and the states listed in table 3. The graphs correspond to the values given in table 5 after normalization to 1 at $\kappa = 0$. Note that four of the six transitions listed in table 3 are of a dipolar character and that the inter-term transitions for $J = 4$ acquire a small forward amplitude, which would be absent without spin–orbit interaction. Figure 4 shows the magnetic intensities for Tm^{3+} as a function of κ for intra- and inter-term transitions. In figures 5 and 6, finally, the theoretical results are displayed together with the experimental values as given in [1, 2].

5. Discussion

We have shown that the energy values derived from our representation of the spin–orbit interaction is in good agreement with measured levels for metallic Pr and Tm. Magnetic neutron scattering is, however, very sensitive to the detailed structure of the eigenstates as they arise from mixing through spin–orbit interaction. Our calculation shows the intensity for the transition to $^3F_4$ in figure 3 to lie slightly above the corresponding value for the transition to $^3F_3$ for $\kappa > 8$ Å^{-1}. This has been demonstrated in [15] to represent a dramatic increase of magnetic intensity for

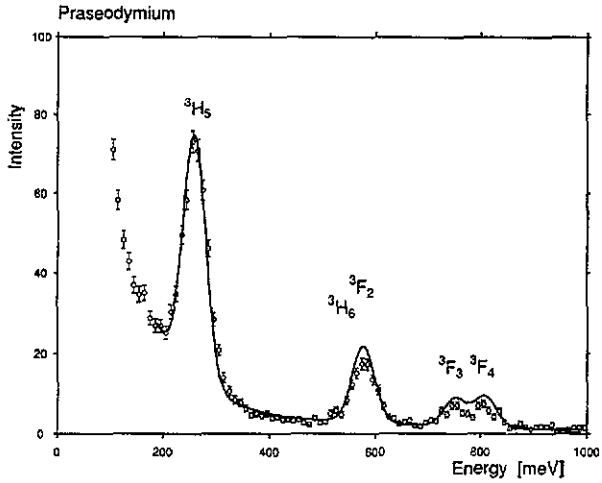

Figure 5. Magnetic intensities for Pr^{3+} are shown together with the measured data. The full curves representing the theory are Gaussians centred at the energies determined from experiment, with half-widths of 25 meV, and with a maximum evaluated from table 5. The curves are labelled by the term dominant in the spin–orbit state.

the this transition compared to the pure LS-state. From figure 3 it is also obvious that the magnetic intensity for the transition to $^3H_6$ is much to weak to be seen in the spectrum in figure 5. With $^3F_2$ and $^3H_6$ both at nearly the same energy—figure 1—the decisive role of the magnetic structure factor in assigning the transition is evident.

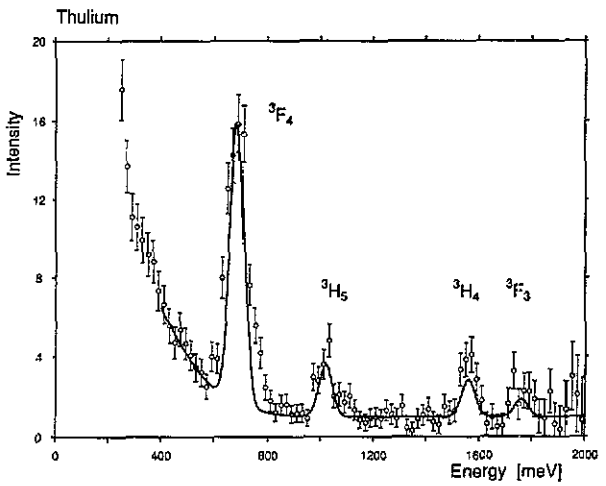

Figure 6. Magnetic intensities are shown together with the measured data. The full curves representing the theory are Gaussians centred at the energies determined from experiment, with half-widths of 25 meV, and with a maximum evaluated from table 5.

For the case of trivalent thulium we see from figure 2 that the state next to the ground state in energy at $\zeta = -327$ meV is, due to level crossing, predominantly of $^3F_4$ character. The corresponding magnetic transition is the most intense—see figure 6—even though it is a non-dipole transition.

Our theoretical analysis confirms the sensitivity of magnetic neutron spectroscopy to the detailed features of magnetic atomic states.

Acknowledgments

One of us, EB, wishes to acknowledge several helpful discussions with R Dirl of the TU Vienna leading to the clarification of the phase dependence of the spin–orbit interaction. The finalization of this paper has been greatly facilitated by travel subsidies granted by the Technical University of Vienna.

References

[1] Osborn R, Balcar E, Lovesey S W and Taylor A D 1991 *Handbook of Physics and Chemistry of Rare Earths* vol 14 ed K A Gschneidner and L R Eyring (Amsterdam: North-Holland)
[2] Taylor A D, Osborn R, McEwen K A, Stirling W G, Bowden Z A, Williams W G, Balcar E and Lovesey, S W 1988 *Phys. Rev. Lett.* **61** 1309
[3] Edmonds A R 1974 *Angular Momentum in Quantum Mechanics* (Princeton, NJ: Princeton University Press)
[4] Judd B R 1963 *Operator Techniques in Atomic Spectroscopy* (New York: McGraw-Hill)
[5] Racah G 1943 *Phys. Rev.* **63** 171
[6] Nielson C W and Koster G F 1963 *Spectroscopic Coefficients for the p^n, d^n and f^n Configurations* (Cambridge, MA: MIT)
[7] Balcar E and Lovesey S W 1988 *J. Phys. C: Solid State Phys.* **21** L1127
[8] Satten R A and Margolies J S 1960 *J. Chem. Phys.* **32** 573
[9] Balcar E and Lovesey S W 1991 *J. Phys.: Condens. Matter* **3** 7095
[10] Balcar E and Lovesey S W 1989 *Theory of Magnetic Neutron and Photon Scattering* (Oxford: Oxford University Press)
[11] Lisher E J and Forsyth J B 1971 *Acta Crystallogr.* A **27** 545
[12] Blume M, Freeman A J and Watson R E 1962 *J. Chem. Phys.* **37** 1245
[13] Brown P J 1992 *International Tables for Crystallography* at press
[14] Freeman A J and Desclaux J P 1979 *J. Magn. Magn. Mater.* **12** 11
[15] Balcar E and Lovesey S W 1992 *Proc. Int. Conf. Neutron Scattering 1991; Physica B* at press